NOVEL WIDEBAND TUNABLE RESONATOR AND THE APPLICATION TO FREQUENCY-AGILE BANDPASS AND BANDSTOP FILTERS

Y.-L. Ma[1, 2], W.-Q. Che[1, *], J.-X. Chen[3], and J.-R. Mao[1]

[1]Department of Communication Engineering, Nanjing University of Science and Technology, Nanjing 210094, China

[2]Faculty of Mathematics and Physics, Huaiyin Institute of Technology, 1 Meisheng Eastern Road, Huaian, Jiangsu 223001, China

[3]School of Electronics and Information, Nantong University, 9 Seyuan Road, Nantong, Jiangsu 226019, China

Abstract—In this paper, a novel end-loaded resonator is investigated and applied to design tunable bandpass filter (BPF) and bandstop filter (BSF). The novelty of the resonator lies in that two varactors are added to the two ends of the resonator, and then its resonant frequency can be bi-directionally tuned. As a result, the theoretical frequency tuning range can be significantly extended to approximately double that of the conventional tunable resonator. For demonstration, the proposed resonator is applied to design tunable BPF and BSF. As expected, the tuning ranges are 52.4% and 53.5% for the BSF and BPF, respectively. Good agreements can be observed between the simulated and measured results.

1. INTRODUCTION

In modern wireless communication systems, tunable frequency filters are often used as tracking filters for multiband telecommunication systems, radiometers, and wide-band radar systems. Therefore, extensive studies have been done and many technologies have been considered in this topic. Different tuning components have been employed in the tunable filter designs, i.e., MEMS switches [1–5], semiconductor varactors [6–17]. Barium-strontium-titanate (BST) [18] and yttrium iron garnet (YIG) techniques [19] are also utilized to design tunable filters.

Among the tunable BPFs, the combline and interdigital structures are widely used as BPFs in modern microwave and millimeter-wave subsystems due to their compactness, excellent stopband and selectivity performance, and easy integration [20]. Microstrip combline and interdigital tunable bandpass filters have been investigated by many researchers in the past few years [1, 2, 6–14]. In recent years, tunable BSFs have attracted increasing interests [4, 15–19]. Regardless of the tuning methods involved in the aforementioned filter designs, the resonators of these filters are each short-circuited to ground or open at the ends while the opposite ends are terminated in lumped capacitors. The using of the abovementioned resonators either limits the tuning range or increases the insertion loss of the filters.

In this paper, a novel end-loaded resonator is investigated and applied to design tunable BPF and BSF. The novelty of the resonator lies in that two varactors are added to the two ends of the resonator, and then its resonant frequency can be bi-directionally tuned. The resonant frequency of the proposed resonator is derived and simulated. As a result, the theoretical frequency tuning range can be significantly extended to approximately double that of the conventional tunable resonator. The demonstrated tunable interdigital BPF with the proposed resonators can achieve a wide tuning range (52.4%) while retaining minimum degradation (less than 2.4 dB) in the passband. The tuning range of the demonstrated tunable BSF using the proposed resonators is 53.5% while the return loss is greater than 10 dB in the tuning range.

2. ANALYSIS OF PROPOSED TUNABLE RESONATOR

Figure 1(a) shows the proposed structure of the resonator loaded by one varactor at one end and another at the opposite end. The transmission line can be either uniform or non-uniform. The analysis is focused on the uniform case. The input admittance Y_{in} is given by

$$Y_{in} = Y_0 \frac{jb_1 + jY_0 \tan \theta_1}{Y_0 + j(jb_1) \tan \theta_1} + Y_0 \frac{jb_2 + jY_0 \tan \theta_2}{Y_0 + j(jb_2) \tan \theta_2} \tag{1}$$

$$b_i = \omega C_{vi} \tag{2}$$

where Y_0 is the characteristic admittance of the transmission line, θ_i the electrical length of the transmission lines, b_i the admittance of the varactors, C_{vi} the tunable capacitance of the varactors, and L ($= \lambda_g/4$, λ_g is the guided wavelength at the resonance frequency) the length of the transmission line. Three typical cases are discussed below.

Case 1: b_1 (or C_{v1}) is infinite and b_2 (or C_{v2}) approaches zero, i.e., the end of the transmission line loaded by varactor (C_{v1}) is equivalently
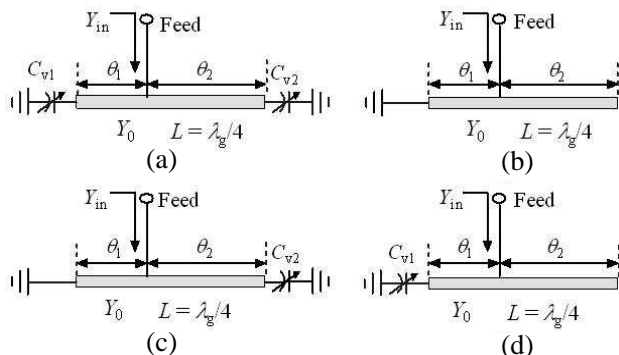
Figure 1. Structure of (a) proposed resonator, (b) conventional quarter-wavelength resonator, (c) resonator shorted at one end, (d) resonator open at one end.

shorted and another end loaded by varactor (C_{v2}) is equivalently open, as shown in Figure 1(b). Thus, the resonant condition is that the imaginary part of Y_{in} is equal to zero, namely, $\text{Im}\{Y_{in}\} = 0$, resulting in

$$\frac{1 - \tan\theta_1 \tan\theta_2}{\tan\theta_1 + \tan\theta_2} = \frac{1}{\tan(\theta_1 + \theta_2)} = 0 \tag{3}$$

Thus, the fundamental resonant frequencies (f_{01}) can be expressed as

$$f_{01} = \frac{c}{4L\sqrt{\varepsilon_e}} \tag{4}$$

c is the velocity of light speed in free space, ε_e is the effective permittivity.

Case 2: b_1 (or C_{v1}) is infinite and b_2 (or C_{v2}) is finite, i.e., the end of the transmission line loaded by varactor (C_{v1}) is equivalently shorted, as shown in Figure 1(c). Similarly, the fundamental resonant frequency (f_{02}) for this case can be derived easily as

$$f_{02} = \frac{[\arctan(Y_0/(2\pi f_{02}C_{V2}))] \cdot c}{2\pi L\sqrt{\varepsilon_e}} \tag{5}$$

When $C_{v2} \approx 0$, meaning the end of the transmission line loaded by varactor (C_{v2}) is equivalently open-circuited, so (5) is equal to (4). It is easy to see that f_{02} may be tuned towards lower frequency as C_{v2} varies from small to large capacitance with the bias voltage (V_2) of the tuned varactor, while the voltage (V_1) of the other varactor (C_{v1}) is fixed, as shown in Figure 2(a).
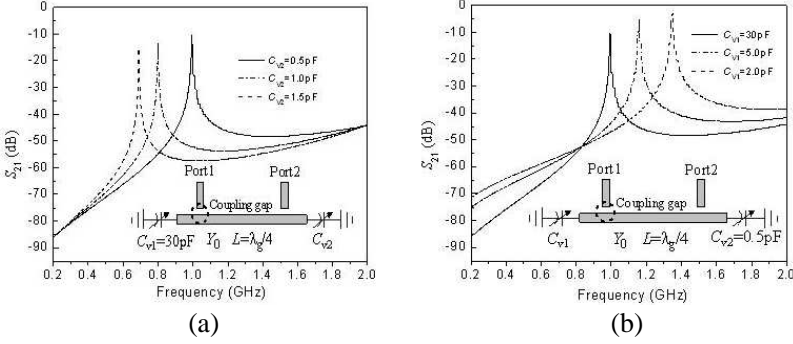
Figure 2. Simulated results of the proposed resonator in Figure 1.
(a) S_{21} versus C_{v2}. (b) S_{21} versus C_{v1}.

Case 3: b_1 (or C_{v1}) is finite and b_2 (or C_{v2}) approaches zero,
i.e., the end of the transmission line loaded by varactor (C_{v2}) is
equivalently open-circuited, as illustrated in Figure 1(d). Similarly, the
fundamental resonant frequency (f_{03}) for this case can be expressed as

$$f_{03} = \frac{[\pi - \arctan(2\pi f_{03} C_{V1}/Y_0)] \cdot c}{2\pi L \sqrt{\varepsilon_e}} \tag{6}$$

When $C_{v1} \to \infty$, implying that the end of the transmission line
loaded by varactor (C_{v1}) is equivalently short-circuited, then (6) is
equal to (4). In this way, f_{03} may be tuned towards upper frequency
as C_{v1} decreases with the reverse-biased voltage (V_1), while the voltage
(V_2) of C_{v2} is kept unchanged, as shown in Figure 2(b).

Based on the above analyses, the proposed resonator can find
some potential applications in tunable filters. For validation purposes,
the filters are implemented using microstrip technology due to the
fabrication simplicity. The substrate used is Rogers RO4000 ($\varepsilon_r =$
3.38, substrate thickness $h = 0.813$ mm, loss tangent $= 0.0027$). The
silicon varactors involved in the designs are ISV232 and JDV2S71E
from Toshiba, and the capacitance ratios of the varactors are 10.5 and
11.5, respectively.

3. DESIGN OF TUNABLE FILTERS USING PROPOSED RESONATOR

3.1. Design of Tunable Interdigital Bandpass Filter

As the coupling coefficients of interdigital structure is larger than
that of combline structure [21], the interdigital filter is easer to be

fabricated and welded with larger coupling space. In this section, a
tunable interdigital BPF is designed to verify the application of the
proposed end-loaded resonators in tunable BPFs. When the ends of the
resonator with C_{v1} (large enough) are equivalently shorted to ground,
the configuration and equivalent circuit of the BPF are shown in
Figures 3(a) and (b). The transmission-line segment is modeled as the
equivalent distributed inductor. The coupling between the resonators
is denoted as the impedance inverter K_{01}. When the ends with C_{v2}
(small enough) are equivalently open-circuited, the configuration and
equivalent circuit of the BPF are shown in Figures 3(c) and (d).
The transmission-line segment (θ_1) is modeled as the capacitor (C_1').
The transmission-line segment (θ_2) and varactor (C_{v1}) are equivalent
to the serial-connected inductor (L) and variable capacitor (C_{v1}').
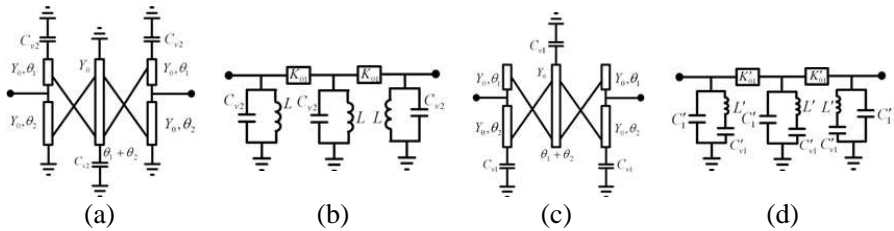
Figure 3. Proposed interdigital BPF. (a) Topology (when C_{v1} is
large enough). (b) Equivalent-circuit (when C_{v1} is large enough).
(c) Topology (when C_{v2} is small enough). (d) Equivalent-circuit (when
C_{v2} is small enough).
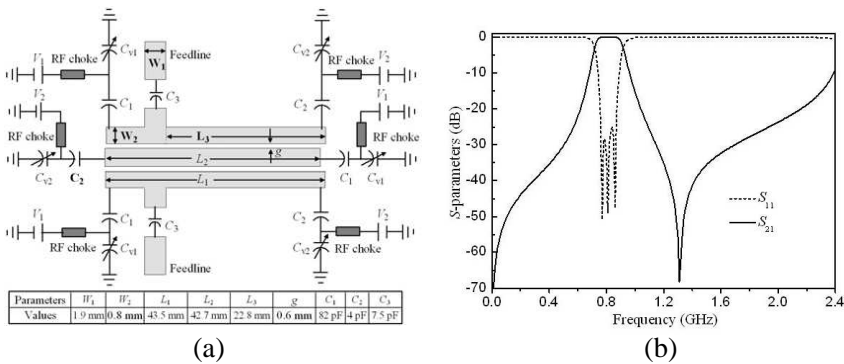
Figure 4. (a) Layout and design parameters of proposed tunable
interdigital BPF. (b) Responses of interdigital BPF without loaded
elements.

The couplings between the resonator lines are also denoted as the impedance inverter K'_{01}.

Figure 4(a) shows the structure and design parameters of the filter using three straight microstrip lines. The input and output feeding lines $(50\,\Omega)$ are tapped at the first and last microstrip lines in which two capacitors (C_3) are embedded and function as DC block. Two different varactors are serially connected at the ends of each microstrip line through the capacitors (C_1 and C_2, functioning as DC block, their selections have been analyzed in [22], and they also service as voltage dividers to give a lower AC voltage swing across the varactors and better linearity). The RF chokes are connected to reduce the impact on the DC power.

In this tunable BPF design, the first step is to design a high performance BPF using the conventional quarter-wavelength microstrip lines as the resonators. The design is similar to that of the interdigital filter [21]. The center frequency of the passband is decided by the length of the microstrip resonator, while the tap position (L_3) and gap (g) affect the external quality factor and coupling coefficient [21]. Therefore, the frequency response may be obtained by choosing appropriate L_3, g and microstrip line length. Figure 4(b) shows the simulated response when $W_1 = 1.9\,\text{mm}$, $W_2 = 1.8\,\text{mm}$, $L_1 = 59.3\,\text{mm}$, $L_2 = 56.3\,\text{mm}$, $L_3 = 42.6\,\text{mm}$, $g = 0.8\,\text{mm}$.

When the ends of the microstrip resonators are end-loaded with the loading elements, as shown in Figure 4(a), the center frequency, external quality factor and coupling coefficient would change. To realize good performance for the filter in the tuning range, C_1, C_2, W_2, L_1, L_2 and L_3 were optimized. The optimized parameters are listed in Figure 4(a). The frequency response of the tunable BPF is discussed as follow.

Initially, the reverse-biased voltage (V_1) of the ISV232 (C_{v1}) is fixed at $0\,\text{V}$, i.e., the capacitance of ISV232 (C_{v1}) is large and the

(a) (b) (c) (d)
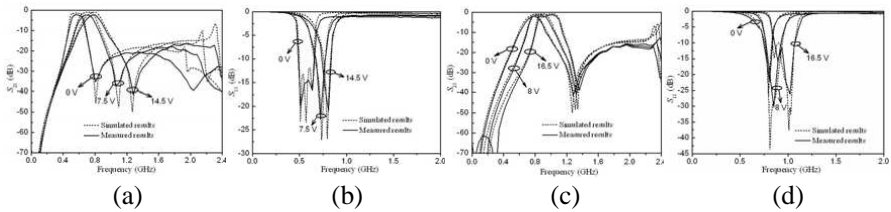
Figure 5. Results for tunable bandpass filter. (a) S_{21} of lower tuning range. (b) S_{11} of lower tuning range. (c) S_{21} of upper tuning range. (d) S_{11} of upper tuning range.

ends with which are equivalently short-circuited. The fundamental passband frequency decreases with the reverse-biased voltage (V_2) of JDV2S71E (C_{v2}) from 14.5 to 0 V (i.e., the capacitance of JDV2S71E (C_{v2}) varies from small to large capacitance). The simulated and measured results in cases of several bias voltages are plotted in Figurea 5(a), (b). The tendency of the tuned frequency in Figures 5(a), (b) corresponds well to that in (5). The center frequency can be continuously tuned from 572.9 to 777.1 MHz (featuring fractional tuning range of 30.3%), while the measured passband insertion loss over the tuning range varies from 2.14 to 2.4 dB, including the loss of the SMA connectors. The passband return loss is better than −12 dB within the tuning range. For each tuning state, a transmission zero is found to locate at the upper edges of the fundamental passband, which improve the roll-off rate.

When the bias voltage (V_2) of the JDV2S71E (C_{v2}) is fixed at 14.5 V, i.e., the capacitance of JDV2S71E is small and the ends connecting JDV2S71E (C_{v2}) are equivalently open-circuited, the fundamental passband frequency increases with the bias voltage (V_1) of ISV232 (C_{v1}) from 0 to 16.5 V (i.e., the capacitance of ISV232 (C_{v1}) varies from large to small). The simulated and measured results for different bias voltages are shown in Figures 5(c), (d), agreeing well with the results from (6). The center frequency can be continuously tuned from 777.1 to 979.3 MHz (23.8%). The measured insertion loss of the passband over the tuning range varies from 2.4 to 1.44 dB. The passband return loss is better than −10 dB within the tuning range. A transmission zero is also located at the upper edges of the fundamental passband within the tuning range, and high selectivity is obtained.

The implemented filter is shown in Figure 6 with the size of $0.21\lambda_g \times 0.07\lambda_g$ (59.3 mm × 19.6 mm), which includes the diodes and the soldering pads, where λ_g is the guided wavelength at the lowest passband frequency. The frequency can be tuned from 572.9 to 979.3 MHz (52.4%) with the insertion loss less than 2.4 dB. For
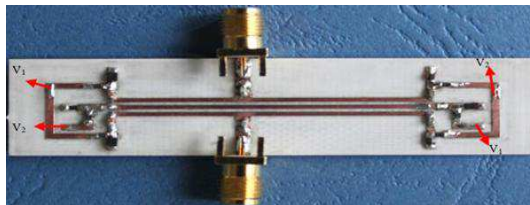
Figure 6. Fabricated prototype of proposed interdigital bandpass filter.

Table 1. Comparisons of several BPFs.

Ref.	Constant bandwith	Size	Loading elements	Tuning range	Maximum insertation loss
[12]	Yes	$0.06\lambda g \times 0.2\lambda g$	Si varactor	18%	$-3.5\,\text{dB}$
[13]	Yes	$> (0.15\lambda g \times 0.13\lambda g$	Si varactor	15%	$\approx -6\,\text{dB}$
[14]	No	$0.25\lambda g \times 0.11\lambda g$	Si varactor	60%	$-5\,\text{dB}$
this work	No	$0.15\lambda g \times 0.07\lambda g$	Si varactor	52.4%	$-3.3\,\text{dB}$
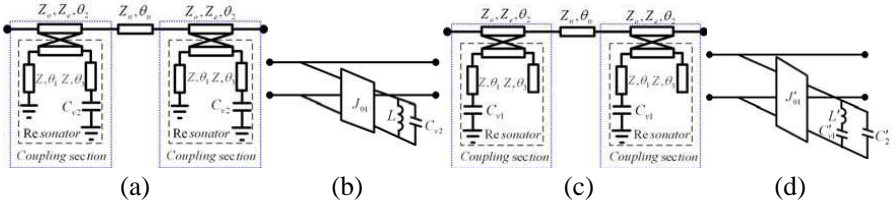
Figure 7. Proposed BSF. (a) Topology (when C_{v1} is large enough). (b) Equivalent-circuit of the coupled-line section (when C_{v1} is large enough). (c) Topology (when C_{v2} is small enough). (d) Equivalent-circuit of the coupled-line section (when C_{v2} is small enough).

comparison, Table 1 summarizes the comparison of the proposed BPF and other work. We may see that the proposed filter has the advantages of compact size, wide tuning range and minimum degradation.

3.2. Design of Tunable BSF

In this section, a tunable BSP is designed to verify the application of the proposed end-loaded resonators in tunable BPFs. When the ends of the resonator with C_{v1} (large enough) are equivalently shorted to ground, the configuration and equivalent circuit of the proposed BPF are shown in Figures 7(a) and (b). The coupling region is denoted by the admittance inverter J_{01}. The resonator is equivalent to the parallel-connected inductor L and capacitor C_{v2}. When the ends with C_{v2} (small enough) are equivalently open-circuited, the configuration and equivalent circuit of the proposed BPF are shown in Figures 7(c) and (d). The transmission-line segment (θ_3) is modeled as the capacitor (C_2'). The transmission-line segment (θ_2) and varactor (C_{v1}) are equivalent to the serial-connected inductor (L') and variable capacitor (C_{v1}'). The coupling between the resonator lines is also denoted by the

admittance inverter J'_{01}.

Figure 8(a) shows the structure and design parameters of the BSF. The basic structure consists of two coupled-line sections and a transmission line in the middle. In each coupled-line section, the resonator is coupled to the main line, forming a bandstop structure. Two capacitors (C_2) are embedded in the feeding lines ($50\,\Omega$) functioning as DC block. The varactors (ISV232) are serially connected at the ends of each resonator directly, while the varactors (JDV2S71E) are serially connected at the opposite ends of each resonator through the capacitors (C_1, functioning as DC block). The RF chokes are connected to reduce the impact on the DC power.

In this tunable BSF design, the first step is also to design a high performance BSF using the conventional quarter-wavelength microstrip lines as the resonators. The design procedures are similar to that of the BSF [21]. Therefore, the frequency response may be obtained by choosing the appropriate length of the microstrip resonator, the length and gap of the coupled-line section. Figure 8(b) shows the simulated response when $W = 1.9\,\text{mm}$, $W_1 = 0.4\,\text{mm}$, $W_2 = 1\,\text{mm}$, $W_3 = 2\,\text{mm}$, $s = 0.2\,\text{mm}$, $L_1 = 17.8\,\text{mm}$, $L_2 = 12.95\,\text{mm}$, $L_3 = 9.2\,\text{mm}$, $L_4 = 0.1\,\text{mm}$, $L_5 = 11.55\,\text{mm}$, $L_6 = 7.8\,\text{mm}$, $L_7 = 3\,\text{mm}$, $L_8 = 2\,\text{mm}$, $L_9 = 5\,\text{mm}$. It is interesting to notice that there are two transmission zeroes in the stopband, owing to the different length of the two resonators. When the ends of the microstrip resonators are end-loaded with the loading elements, the optimized parameters are listed in Figure 8(a).

Following the same way with the aforementioned BPF, Fig-

Parameters	W	W_1	W_2	W_3	S	L_1	L_2	L_3
Values	1.9 mm	0.4 mm	1.0 mm	2.8 mm	0.2 mm	17.8 mm	12.15 mm	8.4 mm
Parameters	L_4	L_5	L_6	L_7	L_8	L_9	C_1	C_2
Values	0.1 mm	11.75 mm	8.0 mm	3.4 mm	2.0 mm	7.6 mm	2.5 pF	200 pF

(a)   (b)
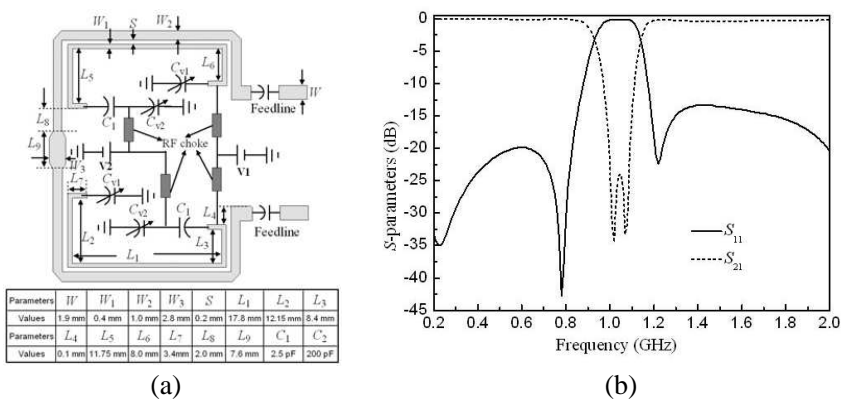
Figure 8. (a) Layout and design parameters of proposed BSF. (b) Responses of BSF without loaded elements.
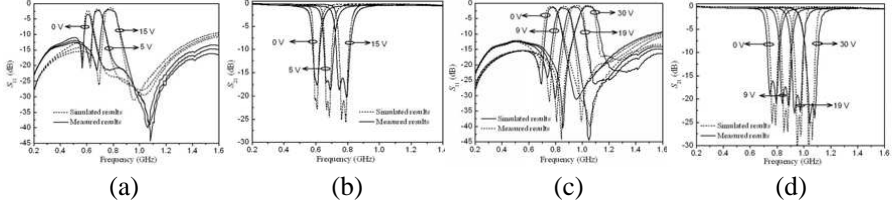
Figure 9. Measured and simulated results for tunable bandstop filter. (a) S_{21} of lower tuning range. (b) S_{11} of lower tuning range. (c) S_{21} of upper tuning range. (d) S_{11} of the upper tuning range.

ures 9(a), (b) illustrates the simulated and measured results for several typical bias voltages (V_2) of JDV2S71E from 15 to 0 V as the reverse-biased voltage (V_1) of the ISV232 (C_{v1}) is fixed at 0 V, which agree fairly with each other. The results show that the fundamental stopband frequency can be continuously tuned from 608.6 to 781 MHz (24.8%). The measured maximum attenuation levels are better than 16.6 dB. The passband insertion loss is better than 0.4 dB, and the return loss is greater than 10 dB for each tuning state. For each tuning state, two transmission poles are near the stopband edges, which improve the roll-off rate.

In the case of the bias voltage (V_2) of JDV2S71E (C_{v2}) fixed at 15 V, the simulated and measured results for several typical bias voltages (V_1) of ISV232 from 0 to 30 V are depicted in Figures 9(c), (d), which are in reasonable agreement. The results show that the fundamental stopband frequency can be continuously tuned from 781 to 1053 MHz (29.6%). The measured maximum attenuation levels are better than 16.6 dB. The passband insertion loss is better than 0.4 dB, and the return loss is greater than 10 dB for each tuning state. Two transmission poles are near the stopband edges, high selectivity is thus obtained. There are two zeroes in the stopband, guarantying the in-band performance.

The implemented filter is shown in Figure 10. The whole size of this filter is less than $0.115\lambda_g \times 0.147\lambda_g$ (30.9 mm × 39.5 mm). The center frequency can be changed from 608.6 to 1053 MHz (53.5%) with the return loss better than 10 dB. A comparison with other reported BSFs is given in Table 2, which shows that the proposed filter using only two unit cells has good characteristics with wide tuning range and better in-band performance.

According to the above descriptions, we can summarize the design procedures of the frequency-agile filters using the proposed tunable resonators as follows.
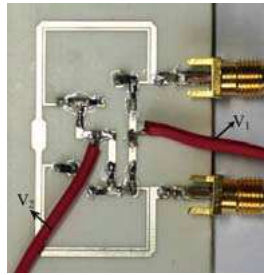
Figure 10. Fabricated prototype of proposed bandstop filter.

Table 2. Comparisons of several BSFs.

Ref.	Constant bandwith	Loading elements	Tuning range	Passband return loss	Passband insertion loss	Stopband attenuation level	Transmission poles	Transmission zezos	Unit cell
[15]	No	Si varactor	25%	<-20 dB	0 dB	<-14 dB	2	2	3
[16]	No	Si varactor	13.2%	-	-	<-20 dB	-	1	1
[17]	Yes	Si varactor	23.9%	<-10 dB	>-2.92 dB	<-55 dB	3	2	6
this work	No	Si varactor	53.5%	<-10 dB	>-0.4 dB	<-16.6 dB	2	2	2

1. First, calculate the physical dimensions of a conventional quarter-wavelength resonator according to the design requirements. Second, with the help of ADS, the initial physical parameters of the filter can be attained. Last, the optimized physical parameters can be achieved by using the EM simulator, e.g., HFSS.

2. Select the suitable loading elements such as the DC block capacitors, the varactors and the chokes according to the frequency response of the above filter using the conventional quarter-wavelength resonators and then add the loading elements to the filter. In order to decrease the insertion loss and obtain a wide tuning range, the capacitance ratio and the resistance of the varactors should be larger and smaller respectively.

3. The structural model is built in the EM simulator such as HFSS and the lumped elements are built in ADS. Through the co-simulation, the frequency response can be attained from the simulation results of ADS. By optimizing the physical dimensions and lumped elements a tunable filter with high performance can be got.

4. CONCLUSIONS

This paper presents a novel tunable resonator, which is end-loaded by two different varactors. The resonant condition is analyzed

and simulated. This kind resonator is employed to design the frequency-agile BPF and BSF. The simulated results and experimental veri?cations have been provided, agreeing well with the theoretical predictions, and also indicates that the filters consisting of the proposed resonators have a wider tuning range than the conventional tunable filters, while retaining better performance, e.g., better passband insertion loss or stopband return loss etc.. For the tunable BPF, a wide tuning range (52.4%) has been achieved with the insertion loss less than 2.4 dB. A transmission zero is near the upper passband edges and the selectivity is improved for each tuning state. With regard to the tunable BSF, a wide tuning range (53.5%) has been achieved with the return loss better than 10 dB. For each tuning state, two transmission poles are near the stopband edges and two transmission zeroes are located in the stopband. With these features, this kind of tunable BPF and BSF using the proposed end-loaded resonators can be very useful in multiband and wideband reconfigurable systems.

ACKNOWLEDGMENT

REFERENCES

1. Li, L. and D. Uttamchandani, "Demonstration of a tunable RF MEMS bandpass filter using silicon foundry process," *Journal of Electromagnetic Waves and Applications*, Vol. 23, Nos. 23, 405–413, 2009.

2. Saha, S. C., U. Hanke, H. Sagberg, T. A. Fjeldly, and T. Saether, "Tunable bandpass filter using RF MEMS capacitance and transmission line," *Progress In Electromagnetics Research C*, Vol. 23, 233–247, 2011.

3. Shalaby, M. M., Z. Wang, L.-W. Chow, B. D. Jensen, J. L. Volakis, K. Kurabayashi, and K. Saitou, "Robust design of RF-MEMS cantilever switches using contact physics modeling," *IEEE Trans. Indus. Electron.*, Vol. 56, No. 4, 1012–1020, 2009.

4. Reines, I., S. J. Park, and G. M. Rebeiz, "Compact low-loss tunable X-band bandstop filter with miniature RF-MEMS switches," *IEEE Trans. Microw. Theory and Tech.*, Vol. 58, No. 7, 1887–1895, 2010.

5. Janardhana, V., S. Pamidighantam, N. Chattoraj, and R. G. Kulkarni, "Experimental investigations on a surface micro-machined tunable lowpass filter," *Progress In Electromagnetics Research Letters*, Vol. 27, 171–178, 2011.

6. Jung, D.-J. and K. Chang, "Accurate modeling of microstrip dumbbell shaped slot resonator (DSSR) for miniaturized tunable resonator and band-pass filter," *Progress In Electromagnetics Research C*, Vol. 23, 137–150, 2011.

7. Yu, F. L., X. Y. Zhang, and Y. B. Zhang, "Frequency-tunable bandpass filters with constant absolute bandwidth and improved linearity," *Progress In Electromagnetics Research Letters*, Vol. 33, 131–140, 2012

8. Wang, Y.-Y., F. Wei, B. Liu, H. Xu, and X.-W. Shi, "A tunable bandpass filter with constant absolute bandwidth based on one ring resonator," *Journal of Electromagnetic Waves and Applications*, Vol. 26, Nos. 11–12, 1587–1593, 2012.

9. Wei, F., L. Chen, X.-W. Shi, and C.-J. Gao, "UWB bandpass filter with one tunable notch-band based on DGS," *Journal of Electromagnetic Waves and Applications*, Vol. 26, Nos. 5–6, 673–680, 2012

10. Liu, B., F. Wei, Q. Y. Wu, and X. W. Shi, "A tunable bandpass filter with constant absolute bandwidth," *Journal of Electromagnetic Waves and Applications*, Vol. 25, Nos. 11–12, 1596–1604, 2011.

11. Wang, S. and R. X. Wang, "A tunable bandpass fillter using Q-enhanced and semi-passive inductors at S-band in 0.18 CMOS," *Progress In Electromagnetics Research B*, Vol. 28, 55–73, 2011.

12. Sánchez-Renedo, M., "High-selectivity tunable planar combline filter with source/load multiresonator coupling," *IEEE Microw. and Wirel. Compon. Lett.*, Vol. 7, No. 7, 513–515, 2007.

13. Kim, B. W. and S. W. Yun, "Varactor-tuned combline bandpass filter using step impedance microstrip lines," *IEEE Trans. Microw. Theory and Tech.*, Vol. 52, No. 4, 1279–1283, 2004.

14. Brown, A. R. and G. M. Rebeiz, "A varactor-tuned RF filter," *IEEE Trans. Microw. Theory and Tech.*, Vol. 9, No. 7, 1157–1160, 2000.

15. Hunter, I. C. and J. D. Rhodes, "Electronically tunable microwave bandstop filters," *IEEE Trans. Microw. Theory and Tech.*, Vol. 30, No. 9, 1361–1367, 1982.

16. Wang, X. H., B.-Z. Wang, H. L. Zhang, and K. J. Chen, "A tunable bandstop resonator based on a compact slotted ground

structure," *IEEE Trans. Microw. Theory and Tech.*, Vol. 55, No. 9, 1912–1918, 2007.

17. Zhang, X. Y., C. H. Chan, Q. Xue, and B. J. Hu, "RF tunable bandstop filters with constant bandwidth based on a doublet configuration," *IEEE Trans. Indus. Electron.*, Vol. 59, No. 2, 1257–1265, 2012.

18. Chun, Y. H., J. S. Hong, P. Bao, T. J. Jackson, and M. J. Lancaster, "Tunable slotted ground structured bandstop filter with BST varactors," *IET Microw. Antennas Propag.*, Vol. 3, No. 5, 870–876, 2009.

19. Tsai, C. S., "Tunable wideband microwave bandstop and bandpass filters using YIG/GGG-GaAs layer structures," *IEEE Trans. Magnetics*, Vol. 41, No. 10, 3568–3570, 2005.

20. Matthaei, G. L., "Combline band-pass filters of narrow or moderate bandwidth," *Microwave J.*, 82–91, 1963.

21. Hong, J. S. and M. J. Lancaster, *Microstrip Filter for RF/Microwave Applications*, Wiley, New York, 2001.

22. Chen, J. X., J. Shi, Z. H. Bao, and Q. Xue, "Tunable and switchable bandpass filters using slot-line resonators," *Progress In Electromagnetics Research*, Vol. 111, 25–41, 2011.